

Digital Object Identifier

Model Predictive Control of Marine Power Plants with Gas Engines and Battery

TORSTEIN I. BØ^{1,3}, ERLEND VAKTSKJOLD², EILIF PEDERSEN³, AND OLVE MO⁴

¹SINTEF Ocean, Otto Nielsens veg 10, 7491 Trondheim, Norway (email: torstein.bo@sintef.no)

²Rolls-Royce Bergen Engines AS, Hordvikneset 125, 5108 Hordvik, Norway, (email:erlend.vaktskjold@rolls-royce.com)

³Norwegian University of Science and Technology - NTNU, at Department for Marine Technology, 7491 Trondheim, Norway (email: eilif.pedersen@ntnu.no)

⁴SINTEF Energy, Sem Sælands vei 11, 7034 Trondheim, Norway (email:olve.mo@sintef.no)

The authors of this paper are partly funded by the SFI Smart Maritime, which is mainly supported by the Research Council of Norway through the Centres for Research-based Innovation (SFI) funding scheme, project number 237917. The authors of this paper are funded in part by the project Optimization of Marine Energy Storage Systems for Desired Lifetime, Energy Saving and Safety, which is primarily supported by the Research Council of Norway, project number 254766.

ABSTRACT The electric load demand on marine vessels is constantly changing during some operational modes, such as in harsh weather or complex operations. Therefore, diesel engines are typically used to handle these variations. Gas engines reduce the CO₂ due to a lower carbon content in LNG compared with diesel oil. However, they may not be able to handle the load variations of a marine power plant. There are multiple other energy sources with strict rate constraints, such as slow speed diesel engines and fuel cells. In such cases, a battery may be used to take care of the variations, while the generator set produces a slowly varying power. In this paper, a common power flow controller for the battery and the generator set is proposed. It utilizes the rotating inertia in the generator set as energy storage, in addition to a battery. This is done by allowing a small excursion in the speed of the generator set, the speed change will change the kinetic energy of the generator set and this is used analogous to an energy storage. The controller is compared with a baseline controller based on virtual inertia and speed-droop. A simulation study is included to demonstrate the performance of the control methods. The simulation study shows that the gas engine (with strict constraints) is not able to handle the given load series. Nonetheless, it can be used in combination with a battery to handle the variations. The power plant can handle a measured load series from a offshore vessel when either speed-droop control or model predictive control (MPC) is used. However, the study indicates that by using MPC, the aging of the batteries and fuel rate variations can be reduced.

INDEX TERMS Energy storage, Gas engine, Predictive control, Power control

I. INTRODUCTION

Marine electric power grids are often subjected to large power variations. These come from variations in, e.g., environmental loads, thruster demands, hotels demand, crane loads and drilling drives [1]. Traditionally, diesel engines and gas turbines have been used to produce power on marine vessels. One of the reasons for this is that they react fast enough to follow load variations, so that the speed and hence the electric frequency, does not vary too much.

The Third IMO Greenhouse Gas Study 2014 estimates that greenhouse gas emissions from marine vessels will increase by 50 to 250%, as measured in CO₂-equivalents, by 2050 for the business as usual scenarios [2]. Yet, it is estimated that the peak in net emissions from shipping needs to peak

by 2025 in order to be able to meet the 2-degree goal [3]. Alternatives to conventional engines may be used to meet this target, such as gas engines and fuel cells. Otto-cycle natural gas engines premix natural gas with air before it is compressed in the cylinder. If the mixture is too lean it will not ignite, resulting in methane slip. Conversely, a mixture that is too rich will autoignite, thus resulting in knocking. Therefore, the engine can only operate in the narrow window between autoignition and misfiring [4]. Load variations make it harder to control the air/fuel-ratio, as the needed fuel will vary. Hence, Otto-cycle natural gas engines are seldom used in diesel electric power plants when the power demand highly varies. The issue of limited dynamic performance is also prominent for engines and alternatives, such as slow speed

diesel engines and proton exchange membrane fuel cells [5]. By combining an Otto-cycle natural gas engine and a battery, the load variations can be handled by the battery, whereas the mean power can be generated by the engines.

In terms of lithium ion batteries, energy storage has already been used in some marine applications. This includes platform support vessels (Edda Ferd [6], Viking Lady [7]), ferries (Prinsesse Benedikte [8], Ampere [9], Tycho Brahe and Tycho Aurora [10]), tugboats (RT Adriaan [11]), high-speed passenger ferries (BB Green [12]) and sightseeing vessels (Vision of the Fjords [13]). The battery packs have many use cases such as: spinning reserve, peak shaving, power smoothing, enhanced dynamic performance, strategic loading and zero emission operation [14], [15].

Variable speed engines have also been suggested for marine power plants. This can be achieved with a direct current (dc) grid, implemented by multiple vendors [9]. With a direct current grid, a rectifier is placed between the synchronous generator and the dc grid. An alternative approach is the "Dynamic AC" concept by ABB [16]. With this concept, the main grid runs with variable frequency ac. Frequency converters are then placed between the grid and each consumer or distribution grid. Both systems allow the generator sets to run at any desired speed, typically from a speed of 70–105%. This provides an opportunity to lower the speed when the power demand is low, as this reduces the specific fuel consumption of the engines. Note that a fixed frequency ac grid is used in this article, which allows the frequency to vary from 5 to 10%.

In this paper, model predictive control (MPC) is used to control the power plant. With MPC, a model of the plant is used to optimize the performance of the plant. The MPC predicts the future state and control trajectory. These trajectories are optimized to minimize the value of the cost function. Because model errors and disturbances may occur, the control optimization problem is solved again at every time step of the controller.

The power demand must be divided between multiple devices when a hybrid power plant is used. This task of splitting the power production between an engine and energy storage is not trivial. MPC is one of the already suggested methods for this task. A combination of battery and ultracapacitors for load smoothing is presented in [17]. The article presents two controllers: One combined control by model predictive control (MPC) of the battery and ultracapacitors. The second controller separates the power variations by a low pass filter and uses two MPCs to individually control the battery and ultracapacitors. An MPC that minimizes the power tracking error or the energy storage losses is presented in [18]. The cost function allows the user to weight the relative importance of energy storage losses and power tracking errors. The controller is demonstrated for a hybrid energy storage consisting of a battery and flywheel and a battery and ultracapacitors. The use of capacitor bank for power smoothing is presented in [19]. The controller uses filtering, in addition to the power available signal, to help regulate the

charging and discharging of the capacitor bank. In [20], a band-pass filter is used to filter out the load variations, which should be canceled. The filter is tuned by an MPC, such that the temperature of the batteries is controlled below an upper limit. In [21], a two-level MPC is used to optimize the performance of a seagoing vessel. An outer MPC is used to optimize the reference trajectory of the propeller shaft speed. This reference is given to an inner MPC, which optimizes the power plant by controlling the power split between the diesel engine, battery and capacitor pack.

The power split problem also arise in other fields. In an island grid, the problem has been studied for a plant with photo voltaic-, wind-, diesel- and battery-systems [22]. The paper presents the control of frequency and voltage by PI- and fuzzy logic controllers. In [23], particle swarm optimization is used to tune PI controllers for frequency regulation of a similar grid. For serial hybrid electric vehicles, heuristics are presented in [24] for the power split between a DC source and battery. The use and control of hybrid energy storage with an ultracapacitor is studied in [25]. Dynamic programming is used to optimize the power split between an internal combustion engine and a battery pack in a series hybrid electric vehicle [26].

This paper presents a combined controller for generator sets and a battery. The purpose of the controller is to utilize the inherent energy storage of the rotating inertia of the generator sets, such that stricter rate constraints can be used on the gas engines, while the use of the battery is reduced. The generator sets have a jump-rate constraint; this is a constraint often used by engine suppliers to keep air/fuel within the operational window. Most port fuel injection engines are capable of a small-scale (± 5 –10%) instant fuel change with no significant fuel/emission cost. Model predictive control is used in this article to control the generator set and battery. Two weight configurations are shown, one which allows a varying frequency (frequency barrier mode) and one with a stiff frequency. A varying frequency reduces the use of the battery by using the rotating inertia of the generator set as an additional energy storage, whereas a stiff frequency can be needed when new generator sets are synchronizing to the grid.

The structure of the paper is as follows: Models of the power plant are presented in the next section. The proposed controller and a baseline controller are presented in Section III. The simulated results are shown in Sections IV and discussed in Section V. Conclusions are then drawn in the last section.

II. MODELS

Two models of the plant are used in this article, the process plant model, used for simulation and the control plant model, used in the controller. The process plant model has the highest fidelity and should capture the most important dynamics of the plant. The control plant model is a simplified model, such that it can be used internally in the controller. An overview of the plant is shown in Figure 1.

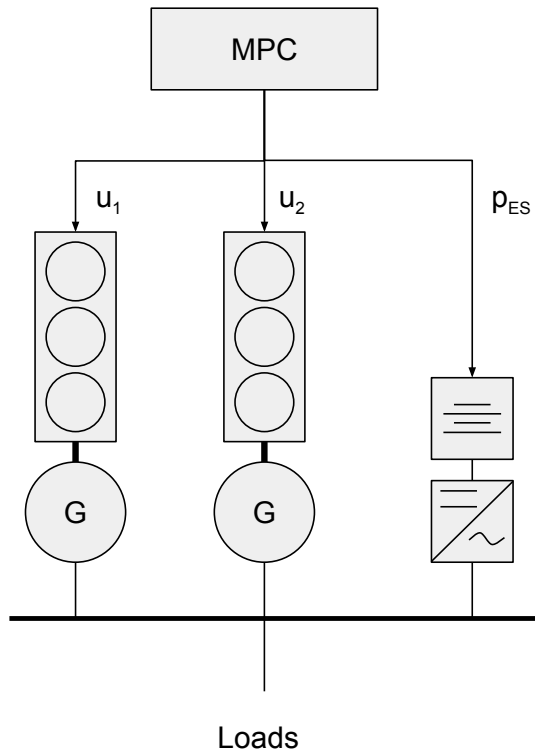


FIGURE 1. Overview of the power plant including the MPC. The MPC commands the fuel rate to the two gas engines, in addition to a charging demand to the battery system. A DC/AC converter is used to control the power between the battery and the main grid, where the two synchronous generators of the gas engines are connected. The power demand is given by a time series.

A. PROCESS PLANT MODEL

As this article only considers the control a power generation and a battery system, the electric power demand is independent of the controller. Therefore, the power plant is simulated, while the power demand is given by a load time series. The load time series is shown in Figure 2, and is previously presented in [27]. This load time series is measured on a platform support vessel of type UT 776 from Rolls-Royce. It has two Rolls-Royce C26:33L9AG gas engines (2.2 MW) and two C26:33L6A diesel engine (2.3 MW). The vessel was in rough weather and dynamic positioning (DP) operation, only running with two gas engines during the measurements. DP operation means that the vessel uses the thrusters to keep its position. The wind speed was 30 knots, and the wave height was three meters.

The setup of the simulated power plant consists of two generator sets of 2 MW each and a battery system, as presented in Figure 1. The electric model of the power plant is presented in [28]. The synchronous generators are modeled by the Behn-Eschenburg model:

$$V_T = E - jX_s I - R_s I \quad (1)$$

where V_T is the terminal voltage, E is the induced voltage in the armature, $x_s = 0.48$ p.u. and $r_s = 0.0019$ p.u. are the

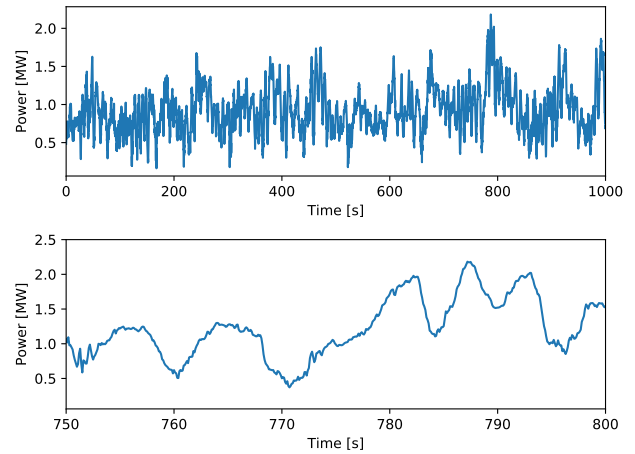


FIGURE 2. Power demand from loads of a PSV vessel. The measurement series is later used in the simulations.

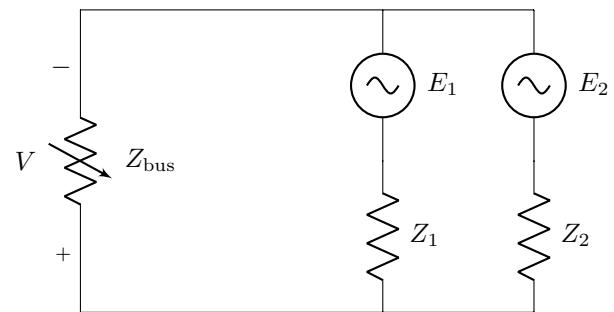


FIGURE 3. Circuit diagram of the power plant.

reactance and resistance of the stator windings and I is the stator current. The battery is modeled as a power source/sink and is subtracted from the consumed power:

$$p_{bus} = p_{load} - p_{battery}. \quad (2)$$

The equivalent model of the power plant is shown in Figure 3. Z_{bus} is calculated such that the power is equal to p_{bus} (see [28] for details).

Per unit variables are used in the article. The per-unit value is given by the absolute value divided by the base value. For instance, $p = \frac{P}{S_b}$, where p is the per-unit power, P is the power in watt and S_b is the base power in watt or volt-ampere. The per-unit values are therefore the value in a percentage of the base value (such as the rated power of the generator set). The base variables are $S_b = 2$ MW, $\omega_b = 60 \times 2\pi$ rad/sec.

The mechanical speed of each generator set is modeled by the torque equation (in per unit):

$$\dot{\omega} = \frac{1}{2H} (\tau_{mech} - D\omega - \tau_{el}) \quad (3)$$

where ω is the per unit rotational speed of the generator set, $H = 3$ seconds is the inertia constant, $\tau_{mech} = u$ is the mechanical torque generated by the fuel burning and $D = 0.1$ is the damping coefficient, which includes mechanical friction

and windage losses. τ_{el} is the electric torque, including active power and electric losses $\frac{p + p_{loss}}{\omega}$.

The engine cannot change the fuel rate, u , too quickly, as this may result in incomplete combustion and large thermal stresses, in addition to Otto-cycle gas engines possibly knocking or misfiring. The generator sets have a jump-rate constraint, which is a constraint often used by engine suppliers to keep air/fuel within the operational window. It is the authors' experience that most port fuel injection engines are capable of small-scale ($\pm 5\text{--}10\%$) instant fuel changes with no significant fuel or emission cost. Figure 4 illustrates this type of constraint. This means that the engine u can jump 0.05 p.u. Furthermore, it is rate constrained with a maximum change of 0.005 p.u. per second. This is implemented by adding a state:

$$\dot{u}_{sat} = \text{sat}_{0.005}(K_{u,sat}(u - u_{sat})) \quad (4)$$

where sat is the saturation function such that $-0.005 \leq \dot{u}_{sat} \leq 0.005$, $K_{u,sat}$ is a gain and should be set to a high value (here 10). The fuel rate is then constrained:

$$u_{sat} - u_{band} \leq u \leq u_{sat} + u_{band} \quad (5)$$

where $u_{band} = 0.05$.

The electric frequency on a marine vessel may vary from $\underline{\omega} = 0.95$ p.u. to $\bar{\omega} = 1.05$ p.u. of rated frequency in steady state [29, Pt. 4, Ch. 8, 1.2.6]. The kinetic energy of the rotating inertia is $\frac{1}{2}J(\omega\omega_b)^2$, where $J = 2HS_b/(\omega_b^2)$. The energy required to spin the generator set from lower to upper frequency limits can therefore be used as an energy storage. The useful kinetic energy storage is thus:

$$E_k = HS_b(\bar{\omega}^2 - \underline{\omega}^2) = HS_b\omega_b(1.05^2 - 0.95^2) \quad (6)$$

For the generator sets used in this study, the useful kinetic energy storage is 333 Wh per generator set, 667 Wh=2.4 MWs in total. Note that the primary advantage of using the rotating inertia as energy storage is the large power rating, while the energy is rather small.

The capacity of the battery is 260 kWh, and it can charge and discharge up to 780 kW. This setup is equivalent to 4 battery packs of type "Power 65" from PBES [30]. The weight of this is 3,800 kg. However, the method is not restricted to batteries, and can also be used with other energy storage solutions such as ultracapacitors and flywheel. A simplified model of the battery is used, as shown in Figure 5. In this simulation, we only consider the power limitations of the battery, losses and aging. The resistance and internal voltage is assumed to be constant. Parameters for the cells are found from a "XALT 75 Ah High Power Superior Lithium Ion Cell" [31]. The internal nominal voltage is $E = 3.7$ V, resistance is $r = 0.71$ m Ω , and the charge capacity of $Q_{battery} = 75$ Ah = 270 kC. Constant parameters are assumed as the variations of SoC is small (less than a few percent). The power of the battery system is:

$$p_{battery} = v_{battery}i_{battery}N_{cell} \quad (7)$$

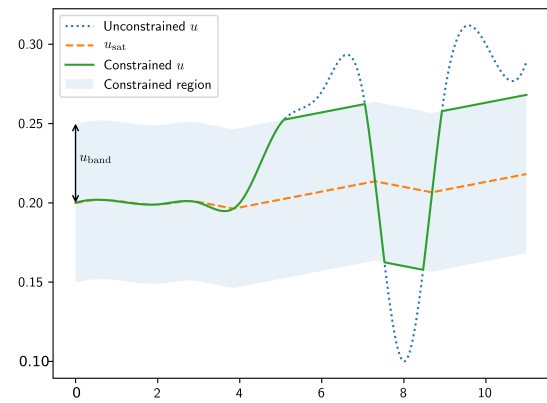


FIGURE 4. Illustration of jump-rate constraint.

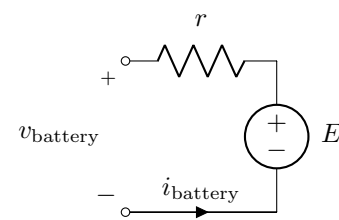


FIGURE 5. Circuit diagram of the battery.

where $N_{cell} = 935$ is the number of cells. The battery system power is limited by the maximum charging power, $-p_{battery}$, and discharge power, $\bar{p}_{battery}$. The power is also limited by the state of charge. The battery cannot be charged if full and discharged if empty. The state of charge is modeled as an integrator:

$$\frac{d\text{SoC}}{dt} = -\frac{i_{battery}}{Q_{battery}} \quad (8)$$

where SoC is the state of charge, $p_{battery}$ is the power delivered by the battery and $Q_{battery}$ is the capacity of the battery. For real applications, voltage limitations will limit the charging power (when the SoC is high) and discharging power (when the SoC is low). This effect is not included, as the simulated state of charge is close to 50%.

A simple model of degrading is given by the number of cycles the cell can withstand. An equivalent full cycle is defined as the absolute energy needed for a complete discharge and charging cycle. For instance, this can be one roundtrip from 100% to 0% and back to 100% SoC, or 10 times 50% to 60% and back to 50% SoC. The number of equivalent full cycles is defined as the integral of:

$$\dot{N}_{cycles} = \left| \frac{d\text{SoC}}{2dt} \right| = \frac{1}{2Q_{battery}} |p_{battery}| \quad (9)$$

The simulated cells are rated to 12,000 cycles and 10 years of operation.

B. CONTROL PLANT MODEL

The control plant model is based on [32], and is used in the MPC. The model assumes that the speeds of the generator sets are close to equal. This happens due to synchronization torque, which keeps the generators at the same frequency. Moreover, damping in the generators (e.g. damping windings and friction) will damp oscillation between the generator sets. The frequency dynamic is derived from the energy balance:

$$\sum_i 2S_{b,i}H_i\dot{\omega}_i = \sum_i S_{b,i} [\tau_{\text{mech},i} - D_i\omega_i - \tau_{\text{el},i}] \quad (10)$$

where subscript i indicates generator set i , and S_b is the base power of the generator set (it converts the per unit power to power).

It is assumed that the frequency is equal for all generators (i.e., $\omega = \omega_i$). In addition, the stator resistance is small. It is therefore assumed that electric losses in the generator are small. This gives: $p_{\text{bus}} \approx \sum_i \tau_{\text{el},i}\omega_i$. The total power on the generators is the difference between the power of the loads and the delivered battery power, $p_{\text{bus}} = p_{\text{load}} - p_{\text{battery}}$. This gives:

$$\left(\sum_i 2S_{b,i}H_i \right) \dot{\omega} = \left(\sum_i S_{b,i}\tau_{\text{mech},i} \right) - \left(\sum_i S_{b,i}D_i \right) \omega - \frac{p_{\text{load}} - p_{\text{battery}}}{\omega} \quad (11)$$

The resistance is neglected in the battery model, so the state of charge is therefore:

$$\frac{d\text{SoC}}{dt} = -\frac{p_{\text{battery}}}{Q_{\text{battery}}EN_{\text{cell}}} \quad (12)$$

III. CONTROLLERS

A. MODEL PREDICTIVE CONTROLLER

A centralized model predictive control (MPC) is used to control both the generator sets and the battery. Model predictive control is a control method based on repeated optimization, with the basis being a cost function and a model of the plant. The MPC predicts a state trajectory for the plant. The cost function puts a cost to the states and control trajectory, such as deviation of the states from the reference value and the cost of using the control inputs. The MPC then optimizes the predicted trajectories so that the cost function is minimized; this optimization may hence be constrained by state and control constraints. The MPC will then implement the first time step in the optimized control trajectory. At the next time instant the optimization problem is solved again with new state measurements, and the newly optimized control input is used. This reoptimization is done at every time step.

An overview of the topology of the plant is shown in Figure 1. The MPC commands the fuel rate to the generator sets, u_{MPC} and power set points to the battery, p_{battery} . The fuel rate, u_{MPC} , is then controlled by the engine, it is assumed that the engine produce a mechanical torque proportional to u_{MPC} . The battery is assumed to be controlled by a power converter, which is able to control the battery power. The task of the

MPC is to keep the frequency within a certain band without violating the constraints of the power plant.

The electric frequency on a marine vessel may vary from 95% to 105% of the rated frequency in steady state [29, Pt.4,Ch.8,1.2.6]. A soft constraint is therefore used to avoid larger frequency variations:

$$\underline{\omega}_{\text{outer}} \leq \omega + s_{\omega,\text{outer}} \leq \overline{\omega}_{\text{outer}} \quad (13)$$

where underbars and overbars indicate lower and upper constraint limits, and s denotes a slack variable. Soft constraints are used to avoid that the optimization problem becomes infeasible when it is not possible to satisfy the constraints. A small safety margin is added to the constraints, which gives $\underline{\omega}_{\text{outer}} = 0.96$ pu and $\overline{\omega}_{\text{outer}} = 1.04$ pu.

In addition, safety functions may reduce the power demand when smaller frequency variations occur [33]. Therefore, an additional inner soft frequency constraint is added:

$$\underline{\omega}_{\text{inner}} \leq \omega + s_{\omega,\text{inner}} \leq \overline{\omega}_{\text{inner}} \quad (14)$$

This makes it possible to use the inertia of the engines for energy storage. The frequency may then travel freely between $\underline{\omega}_{\text{inner}} = 0.97$ p.u. and $\overline{\omega}_{\text{inner}} = 1.03$ p.u. Figure 6 illustrates the frequency cost function.

The battery is constrained by a maximum power and state of charge (SoC) range:

$$p_{\text{battery}} \leq p_{\text{battery}} \leq \overline{p_{\text{battery}}} \quad (15)$$

$$\underline{\text{SoC}} \leq \text{SoC} \leq \overline{\text{SoC}} \quad (16)$$

A cost on deviation from the reference state of charge, SoC_{ref} is included. This is done to make sure that the battery is not discharged or charged over the long term, whereas the SoC at the end of the simulation is equal or close to the SoC at the beginning of the simulation.

The generator set is jump rate constrained. Note that (4) is not smooth due to the saturation function, which may cause numerical problems for the solver. The saturation function is therefore approximated by the hyperbolic tangent function:

$$\text{sat}_a(x) \approx a \tanh\left(\frac{x}{a}\right) = a \left[\frac{2}{1 + e^{-\frac{2x}{a}}} - 1 \right] \quad (17)$$

This gives

$$\dot{u}_{\text{sat}} = \dot{u}_{\text{sat,max}} \left[\frac{2}{1 + \exp\left(\frac{-2K_{u,\text{sat}}(u - u_{\text{sat}})}{u_{\text{sat,max}}}\right)} - 1 \right] \quad (18)$$

where $\dot{u}_{\text{sat,max}} = 0.005$. Furthermore, the constraint on the fuel rate is:

$$u_{\text{sat}} - u_{\text{band}} \leq u \leq u_{\text{sat}} + u_{\text{band}} \quad (19)$$

The generator set limits must also be enforced:

$$\underline{u} \leq u \leq \overline{u} \quad (20)$$

These are hard constraints, since they are the physical limits of the generator. The controller optimizes the time derivative

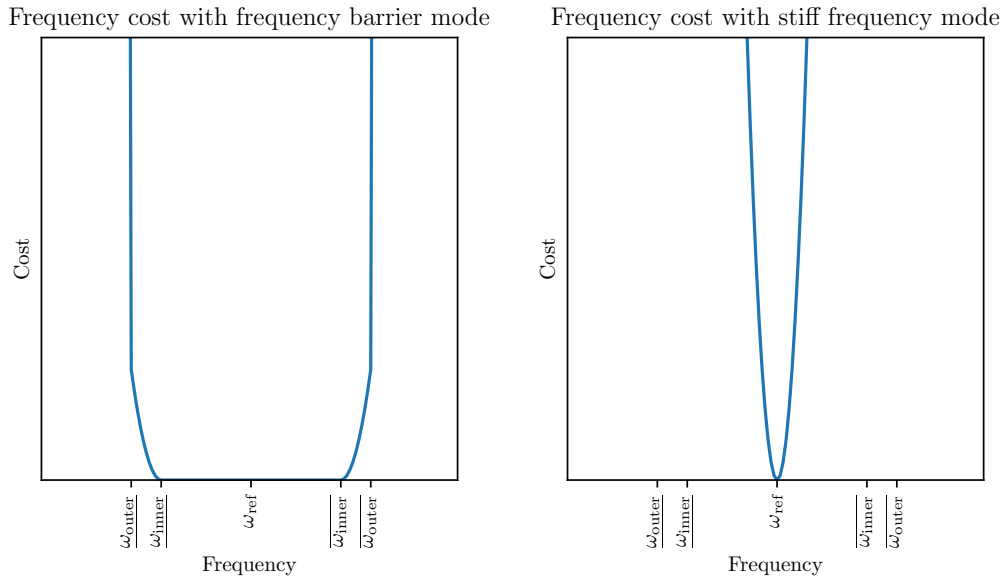


FIGURE 6. Frequency cost function with the two configurations of the cost function. For the frequency barrier mode, the frequency is cheap as long as it is between $\underline{\omega}_{\text{inner}}$ and $\bar{\omega}_{\text{inner}}$, gets more expensive if it goes outside this range. A high cost is added if the frequency goes outside of $\underline{\omega}_{\text{outer}}$ and $\bar{\omega}_{\text{outer}}$. For the stiff frequency mode, the cost of deviating from ω_{ref} is high.

of the fuel rate, \dot{u} . The fuel rate can therefore be found by integration.

The power demand comes in as a disturbance term in equation (11). This means that a prediction of the power demand is needed for the optimization problem. In this article, two types of power predictions are used: low/high predictions and perfect predictions. The *perfect prediction* uses the actual future power demand in the predictions. This is a benchmark test, as the given MPC cannot perform better than with true knowledge of the actual future load. However, the power demand of a marine vessel is hard to predict, and contains some randomness. Hence, a second type of prediction called *low/high prediction* is used in this article. The low/high prediction uses two power scenarios to handle the uncertainties of the future power demand. The two scenarios are a constant high load and a constant low load. An example of power predictions used in the MPC is given in Figure 7. The use of two power scenarios is previously suggested by, for instance [34]. The levels are set to the minimum and maximum load, averaged over 0.5 seconds during the last 10 seconds. Therefore, two sets of predictions for the plants states and control input are used, one for each power scenario, as shown in state predictions in Figure 8. The task of the MPC is then to find a common control input for the two scenarios, such that the constraints are satisfied and the cost is minimized. Since more information is available in the future (e.g. frequency measurements), only the first $N_{\text{common}} = 2$ control inputs must be common. After that period the control inputs for the two scenarios can diverge. As a result, the control inputs are constrained to be equal during the N_{common} first steps in the prediction horizon, for

$$i = 0, 1, 2, \dots, N_{\text{common}} - 1:$$

$$u_1^{\text{low}}(t[k+i]) = u_1^{\text{high}}(t[k+i]) \quad (21)$$

$$u_2^{\text{low}}(t[k+i]) = u_2^{\text{high}}(t[k+i]) \quad (22)$$

$$p_{\text{battery}}^{\text{low}}(t[k+i]) = p_{\text{battery}}^{\text{high}}(t[k+i]) \quad (23)$$

where a superscript low and high denotes the control variables for the low and high power demand predictions. t_k is the time step at the beginning of the prediction. The controller becomes more conservative as N_{common} increases. However, the frequency for the low and high power estimate will diverge with time. A too large N_{common} will give frequencies predictions that eventually violate the frequency barrier. N_{common} is set to 2, as this is a trade-off between performance and conservatism.

The cost function for one scenario (either low power prediction, high power prediction or perfect power prediction) and time step is:

$$\begin{aligned} J(t) = & k_{\omega} (\omega(t) - \omega_{\text{ref}})^2 \\ & + k_{\text{SoC}} (\text{SoC}(t) - \text{SoC}_{\text{ref}})^2 \\ & + k_{p,\text{battery}} (p_{\text{battery}}(t))^2 \\ & + k_{\dot{u},1} (\dot{u}_1(t))^2 + k_{\dot{u},2} (\dot{u}_2(t))^2 \\ & + k_{\text{asym}} (u_1(t) - u_2(t))^2 \\ & + k_{s,\omega,\text{inner}} (s_{\omega,\text{inner}}(t))^2 \\ & + k_{s,\omega,\text{outer}} (s_{\omega,\text{outer}}(t))^2 \end{aligned} \quad (24)$$

where k are weights. The terms are explained in Table 1.

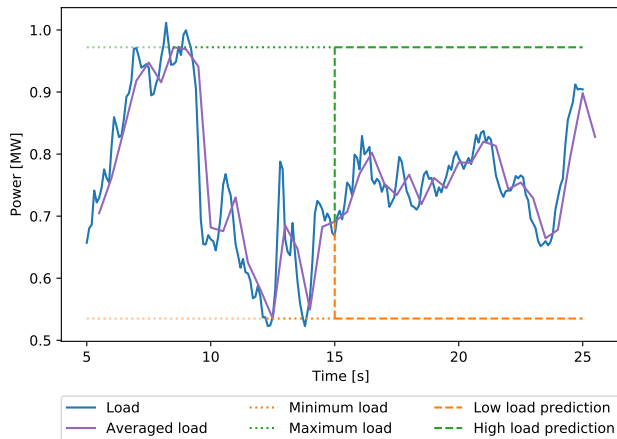


FIGURE 7. Prediction of the future power demand. A high and a low estimate is used. This is done by calculating the average load during one sample period (0.5 seconds); then the minimum and maximum load for the previous 10 seconds is found. This is set as the predicted low and high load.

A terminal cost is also included:

$$J_N(t) = k_{\omega, N} (\omega(t) - \omega_{\text{ref}})^2 + k_{\text{SoC}, N} (\text{SoC}(t) - \text{SoC}_{\text{ref}})^2 \quad (25)$$

The total cost function is:

$$\Phi = \sum_{i=0}^{N-1} [J^{\text{low}}(t[k+i]) + J^{\text{high}}(t[k+i])] + J_N^{\text{low}}(t_{k+N}) + J_N^{\text{high}}(t_{k+N}) \quad (26)$$

The optimization problem is:

$$\begin{aligned} & \min_{\dot{\omega}^{\text{low}}, p_{\text{battery}}^{\text{low}}, \dot{\omega}^{\text{high}}, p_{\text{battery}}^{\text{high}}} \Phi \\ & \text{such that (11 - 23)} \\ & \omega^{\text{low}}(t_k) = \omega^{\text{high}}(t_k) = \omega^i \\ & \text{SoC}^{\text{low}}(t_k) = \text{SoC}^{\text{high}}(t_k) = \text{SoC}^i \\ & u_1^{\text{low}}(t_k) = u_1^{\text{high}}(t_k) = u_1^i \\ & u_2^{\text{low}}(t_k) = u_2^{\text{high}}(t_k) = u_2^i \end{aligned} \quad (27)$$

where N is the length of the prediction horizon, and ω^i , soc^i , u_1^i , and u_2^i are initial values at the current time step.

Two different configurations of weights are used in the cost function. The first configuration, the *frequency barrier mode*, uses a low cost on frequency variations, but large on the use of the battery. This configuration can be used to avoid unnecessary use, and hence cycling, of the battery. The second configuration, the *stiff frequency mode*, uses a high cost on frequency variations, but a low cost on using the battery. This can be used when a constant frequency is needed, for example for an easier synchronization of additional generator sets.

As is normally done with MPC, the first control input in the prediction horizon from (27) is used. At the following time step, equation (27) is reoptimized with new initial conditions.

The MPC is implemented in ACADO using the code export functionality [35]. The prediction horizon, N , is set to 20 samples, with a sampling time of 0.5 seconds. The optimization problem consists of 200 optimization variables and 209 constraints. ACADO solves the optimization problem as a sequential quadratic problem. The computational time is approximately 15 to 60 ms, and with an Intel Xeon CPU E4-1245 3.5 GHz processor, the computational time depends on the number of needed SQP iterations. The controller is therefore able to run in real-time.

B. BASELINE CONTROLLER: SPEED-DROOP AND VIRTUAL SYNCHRONOUS MACHINE

A baseline controller is used to compare the response of the MPC with the response from commonly used speed-droop controller for the generator set and a power smoothing controller for the battery based on virtual inertia and frequency recovery.

1) Speed-droop Control

A speed-droop controller calculates a set-point for the frequency based on the measured power of the generator:

$$\omega_{\text{set}} = \omega_{\text{no-load}}(1 - p \text{ Droop}) \quad (28)$$

where $\omega_{\text{no-load}} = 1.01$ is the no-load frequency and $\text{Droop} = 0.02$ is the speed-droop gain. Note that in many marine power plants compensated droop is used. This outer controller adjusts the no-load frequency, such that the frequency is kept closer to the nominal frequency. This is not included in the current implementation, but can easily be included.

The reference frequency is given to a PID controller, which sets the fuel rate:

$$u = K_P(\omega_{\text{set}} - \omega) + K_I \int (\omega_{\text{set}} - \omega) dt + K_D \hat{\omega} \quad (29)$$

where K_P , K_I , K_D are control gains given in Table 2. $\hat{\omega}$ is an estimate of the time derivative of the generator sets frequency, and it is calculated by dirty derivatives (also known as bandlimited derivatives).

2) Battery Controller

A virtual generator is used, in addition to a frequency recovery method to control the battery. To avoid frequency variations, the battery is controlled to act as a free spinning synchronous generator with no losses. This is done by modeling a virtual generator, using the same models as for the generator sets, i.e., equation (1). The calculated power of the virtual generator is delivered by the battery. When the electric frequency of the grid decreases the load on the modeled generator will increase, as the load angle of the modeled generator increases. This modeled load is then commanded to the battery system. This modeled rotating mass will decrease its speed as the electric torque is applied on the shaft, while the opposite occurs when the frequency increases. Virtual generator control holds the proven properties of synchronous

TABLE 1. Weights in cost function.

		Cost weight	
		Frequency barrier mode	Stiff frequency mode
k_{ω}	$(\omega - \omega_{ref})^2$	10^{-4}	10^4
k_{SoC}	$(SoC - SoC_{ref})^2$	10^4	10^{-1}
$k_{p,battery}$	$p_{battery}^2$	10^4	10^{-1}
$k_{i,1}$	$i_{1,1}^2$	10^7	100
$k_{i,2}$	$i_{1,2}^2$	10^7	100
k_{asym}	$(u_1 - u_2)^2$	10	10
$k_{s,\omega,inner}$	$s_{\omega,inner}^2$	10^7	10^4
$k_{s,\omega,outer}$	$s_{\omega,outer}^2$	10^{10}	10^6
$k_{\omega,N}$	$(\omega - \omega_{ref})^2$	10^8	10^8
$k_{SoC,N}$	$(SoC - SoC_{ref})^2$	10^7	10^3

Cost of deviation from the electric frequency reference
 Cost of deviation from the state of charge reference
 Cost of using power from the battery
 Cost of changing the fuel rate position of engine 1
 Cost of changing the fuel rate position of engine 2
 Cost of asymmetric fuel rate position on engine
 Cost of frequency deviation outside of ω_{inner} and ω_{inner}
 Cost of frequency deviation outside of ω_{outer} and ω_{outer}
 Cost of deviation from the electric frequency reference at end of the prediction horizon
 Cost of deviation from the state of charge at end of the prediction horizon

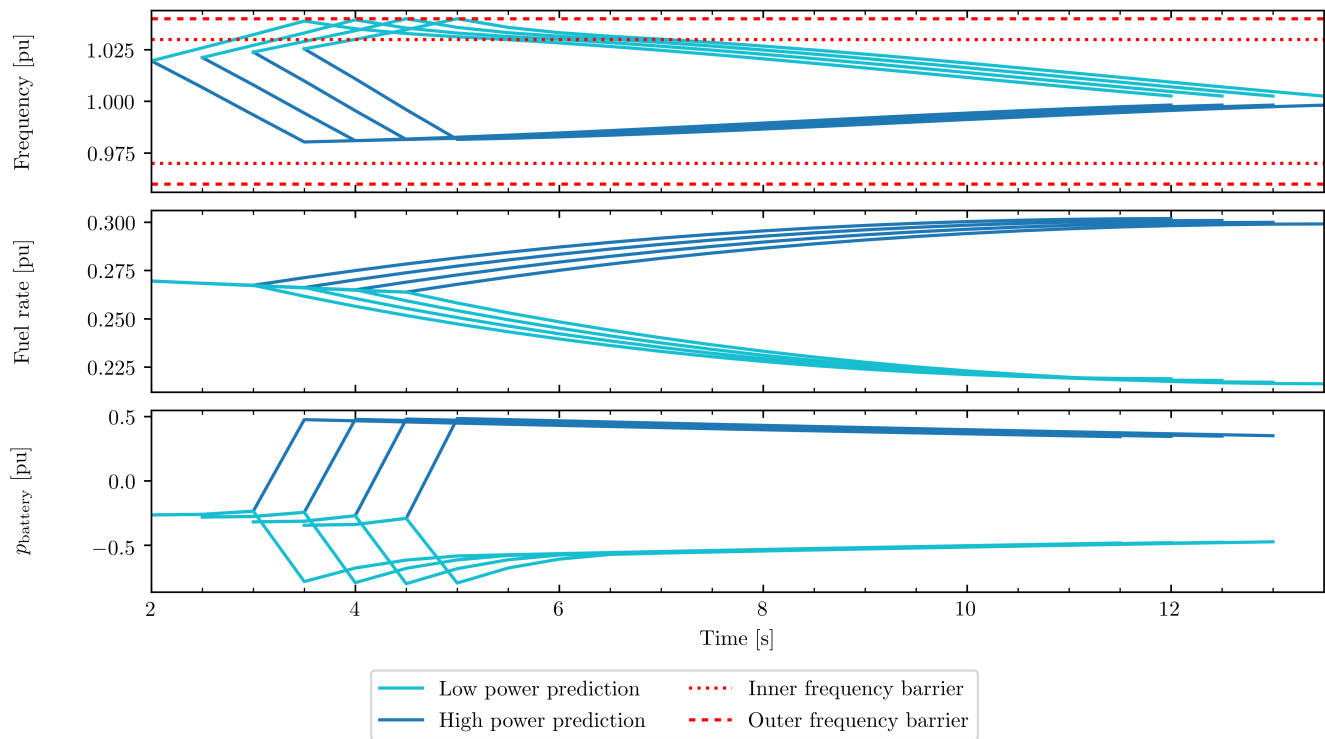


FIGURE 8. Four consecutive predictions from the MPC. The plots show the two different predictions, one for a low power demand and one for a high power demand. Note that the predicted control inputs (fuel rate and power from the battery) are equal for both predictions at the beginning of the horizon. The sampling time is 0.5 seconds.

generators and distributes the control, as the controller only needs to know the voltage of the grid [36]–[38].

A dead-band controller is used for an additional battery power flow to avoid both under- and over frequency. If the frequency goes under a given limit, $\underline{\omega}_r$, the battery discharges. Similarly, if the frequency is above a given limit, $\overline{\omega}_r$, the battery charges:

$$p_{\text{battery},\omega} = \begin{cases} K_{\omega_r}(\overline{\omega}_r - \omega) & \overline{\omega}_r < \omega \\ 0 & \underline{\omega}_r \leq \omega \leq \overline{\omega}_r \\ K_{\omega}(\omega_r - \omega) & \omega < \underline{\omega}_r \end{cases} \quad (30)$$

where K_{ω} is the control gain. The constants are set to $\underline{\omega}_r = 0.97$, $\overline{\omega}_r = 1.03$ and $K_{\omega_r} = 50$. The controller is tuned, such that it is not activated if the frequency follows the droop curve.

The virtual mass and the dead-band controller do not control the state of charge (SoC). To avoid a drift of SoC, a P-regulator is used to regulate the average SoC close to the reference SoC:

$$p_{\text{battery,SoC}} = K_{\text{SoC}}(\text{SoC} - \text{SoC}_{\text{ref}}) \quad (31)$$

In total, the battery power is:

$$p_{\text{battery}} = p_{\text{battery,gen}} + p_{\text{battery},\omega} + p_{\text{battery,SoC}} \quad (32)$$

In addition, p_{battery} is constrained within the power limits of the battery, and set to zero when the power demand would give over- or undercharging.

TABLE 2. Gains used in the baseline controller

	Frequency barrier mode	Stiff frequency mode
Governor K_P	0.1	100
Governor K_I	0.1	5
Governor K_D	10	500
Virtual SM H	N/A	20 s
Virtual SM S_b	0	200 MW

C. TUNING

The baseline controller is implemented with two sets of configurations, frequency barrier and stiff frequency. For the frequency barrier, the system is tuned such that the frequency can travel between the lower and higher frequency. The gains of the governor are tuned with low gains, giving a more "relaxed" response. Moreover, only the dead-band strategy for the battery is used and not the virtual synchronous machine. For the stiff frequency mode, the gains of the governor are high, which gives an aggressive governor. In addition, the virtual generator is used with a large mass and base power. Note that the base power of the virtual synchronous machine is much larger than the maximum power of the battery system, hence the power is limited by the battery. Both configurations are tuned to be as close to the performance of the MPC as possible, with the gains given in Table 2.

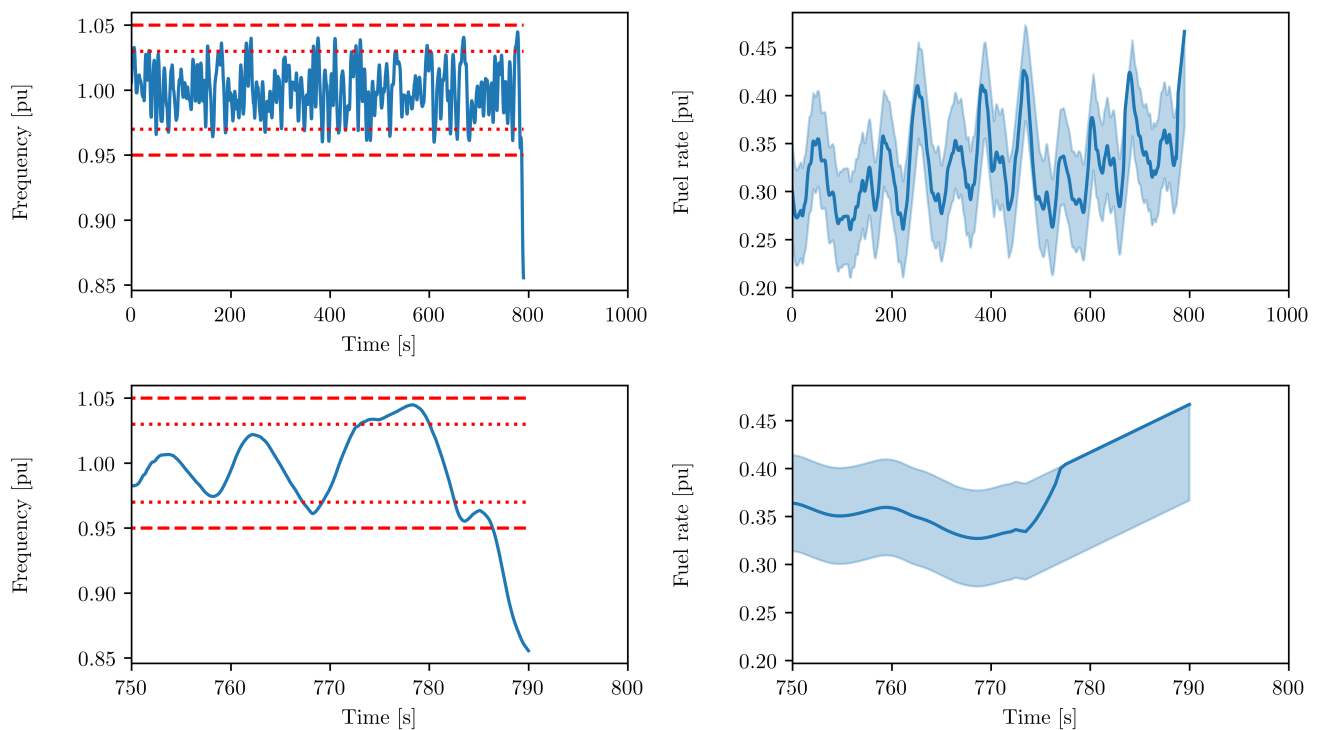


FIGURE 9. Response of the power plant without battery when using the MPC with frequency barrier mode and perfect power predictions. The upper plot shows the result of the 790 first seconds, while the lower plots are zoomed-in on the last 50 seconds.

IV. RESULTS

Figure 9 shows the results of a simulation without the use of the battery, which is done to check whether the battery is needed. The MPC controller is used with perfect predictions and the frequency barrier mode. The frequency drops below 90% after 790 seconds, which would then lead to a blackout. This happens as the load increases after approximately 780 seconds (see Figure 2). However, the controller reacts by increasing the frequency (above the inner frequency barrier) at 773 seconds to increase the kinetic energy. Later on, the fuel rate is increased at 778 seconds. Unfortunately, this is not sufficient, as the frequency drops more than the allowed transient frequency variations of $\pm 10\%$ [29]. Hence, with such strict constraints, the gas engines would not be able to handle the load variations without a battery system. Note that for the actual vessel, where the load series was measured, the gas engines *were* able to handle the load variations, then with more relaxed fuel rate constraints.

Figures 10–16 show the response of the simulation using the power demand from Figure 2. The initial state of charge for the MPC configurations is set such that the initial and terminal state of charge is equal. The upper left plot shows the electric frequency of the grid. The red dashed lines show the $\pm 5\%$ limit given for steady state load variation limits in [29], while the red dotted lines show the band for the inner frequency limits for the MPC. The region between the dotted lines is the region that the frequency can freely travel, as set by the cost function. The middle left plot shows the fuel rate

of the engine, and the shaded region is the allowed region given by the jump-rate constraint. The lower left plot shows the time derivative of the fuel rate, whereas the upper right plot shows the power delivered by the battery. The middle right plot shows the state of charge of the battery, while the lower right plot shows the accumulated number of equivalent full cycles for the battery.

In Figures 10 and 11, the response of the power plant is shown when the baseline controller is used. For the stiff frequency (Figure 10), it is seen that the battery takes most of the variations. At 780 seconds, the battery and engines are not able to deliver sufficient power, so a small drop in frequency occurs. The frequency has a small deviation from the rated frequency; this occurs due to the use of a speed-droop and can be avoided by compensated droop. The spikes in the change of fuel rate is due to rapid changes of the load, which the droop controller reacts on. The frequency barrier mode (Figure 11) reduces the battery usage, by letting the frequency vary between the higher and lower frequency limits. Nevertheless, some high frequency load variations are still seen in the fuel rate of the gas engines.

In Figures 14–16, the result of using the stiff frequency mode is presented. Note that the frequency is not kept close to the reference frequency when the low/high predictions are used in Figure 15. To increase the performance, the sampling rate is increased to 10 Hz; consequently, the frequency is much closer to the reference frequency, as shown in Figure 16.

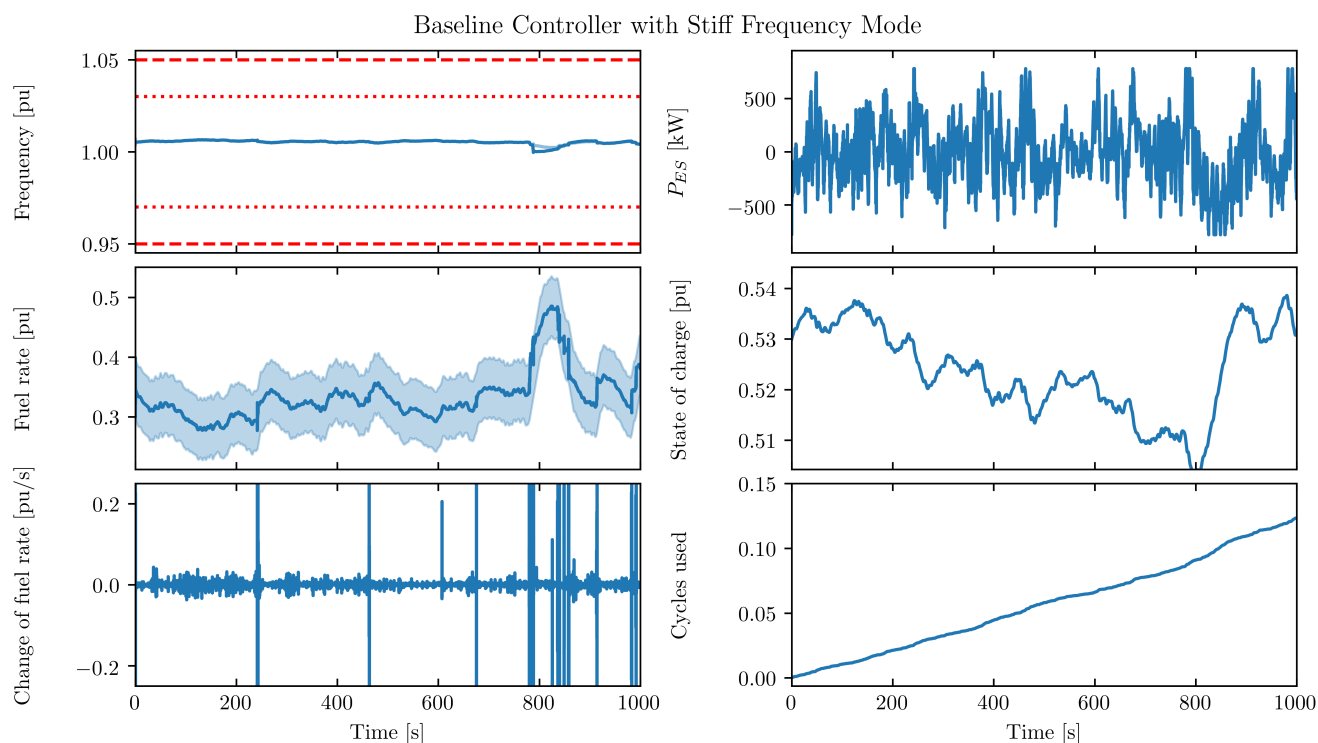


FIGURE 10. Response of the power plant when using the baseline controllers and stiff frequency mode. The light line in the frequency plot (upper left) shows the reference frequency given by the droop curve.

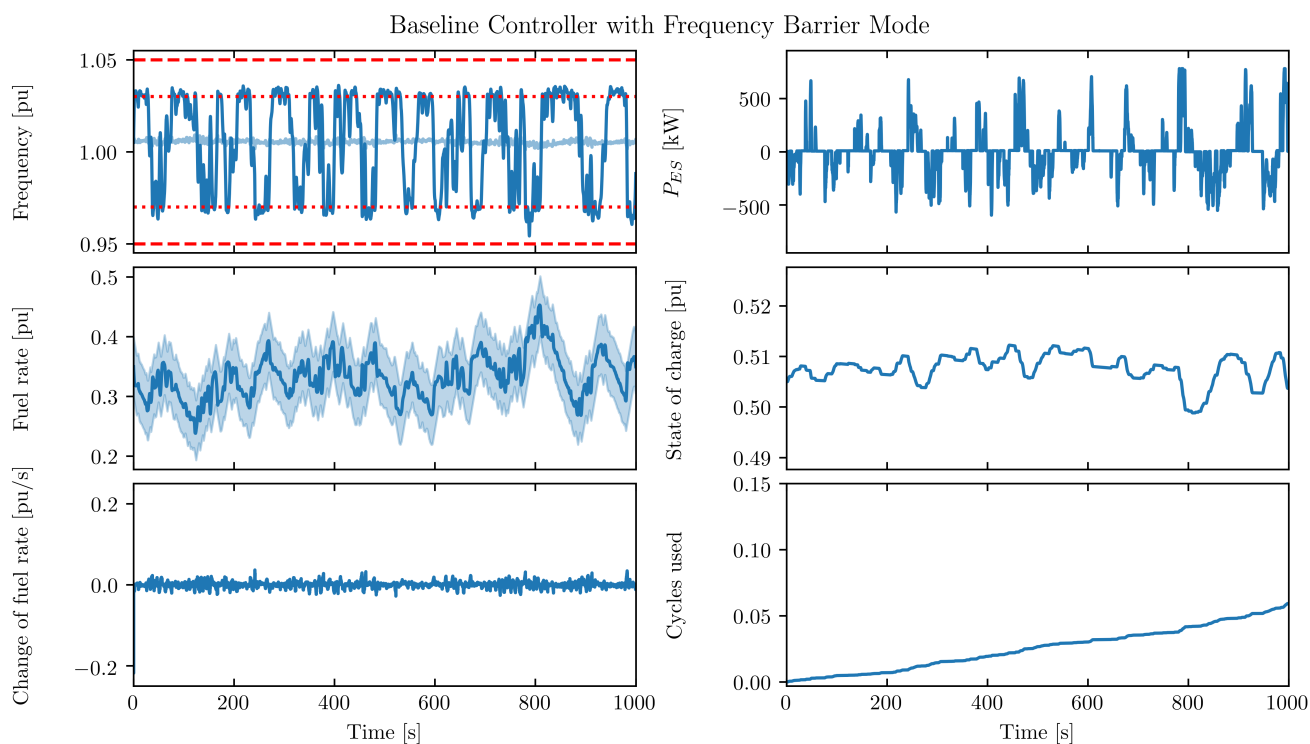


FIGURE 11. Response of the power plant when using the baseline controllers and frequency barrier mode. The light line in the frequency plot (upper left) shows the reference frequency given by the droop curve.

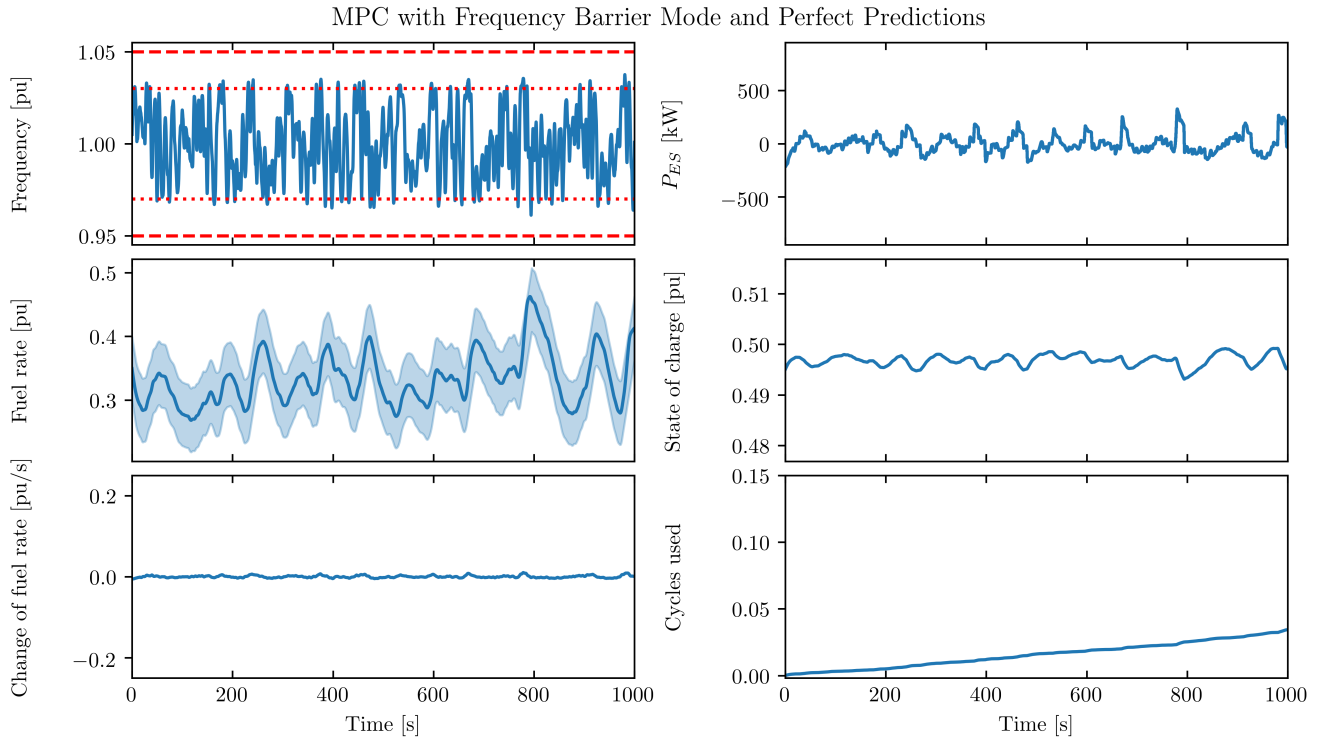


FIGURE 12. Response of the power plant when using the MPC with frequency barrier mode and perfect predictions

TABLE 3. The table shows the number of equivalent full cycles the battery is cycled if the load series is repeated for 10 years. The batteries are expected to last for 10 years, and withstand 12,000 cycles. The energy loss in the battery is also included in the table. It is given as the ratio between lost energy in the battery due to ohmic losses and the total consumed energy by the consumers. The root mean square of \dot{u} is shown in the right-hand column.

Mode	Cycles after 10 years	Energy loss	RMS \dot{u} [%/s]
Frequency barrier, baseline	18,684	0.2%	0.77
Stiff frequency, baseline	38,968	0.5%	30
Frequency barrier, perfect prediction	10,920	0.04%	0.28
Frequency barrier, low/high prediction	28,032	0.3%	0.37
Stiff frequency, perfect prediction	29,136	0.3%	0.32
Stiff frequency, low/high prediction	39,672	0.5%	0.75
Stiff frequency, low/high predictions, 10 Hz	39,000	0.5%	0.28

The resulting cycling is shown in Table 3. It shows the number of equivalent full cycles if this load series was continuously repeated for 10 years.

V. DISCUSSION

A. BASELINE CONTROLLER VS. MPC

The baseline controller gives an acceptable response. For the stiff frequency mode, the frequency is kept at a constant frequency, with the exception of one frequency deviation due to a load increase. The frequency barrier mode reduces the

use of the battery, while keeping the frequency within the given limits.

However, the MPC can improve the performance further. For the stiff frequency mode, the MPC can reduce the variations of the fuel rate significantly, both for perfect predictions and low/high predictions, with a 10 Hz sampling frequency. In addition, if perfect predictions are available, the number of equivalent cycles is reduced by 25% and the frequency deviation is avoided.

For the frequency barrier mode, variations in the fuel rate are reduced by using MPC. If perfect predictions are available, the number of equivalent cycles is reduced by 41%.

Note that the baseline controller uses distributed control, whereas the MPC is centralized. Reliability is highly important for vessels with dynamic positioning system. The disadvantage with a centralized controller is that the system is vulnerable to a single failure in the main controller, so distributed control schemes are therefore often preferred. Thus, a backup controller may be used in cases where the MPC fails. For example, this can be the suggested baseline controller with the stiff frequency mode. The battery can also implement the dead-band controller, which discharges if the frequency is too low or charges if the frequency is too high. This will distribute some safety functions. Yet, it should be noted that a distributed system may also fail. For instance, a locked fuel rate on an engine may cause an overload or reverse power. Hence, reliability is a concern for both distributed and centralized control schemes.

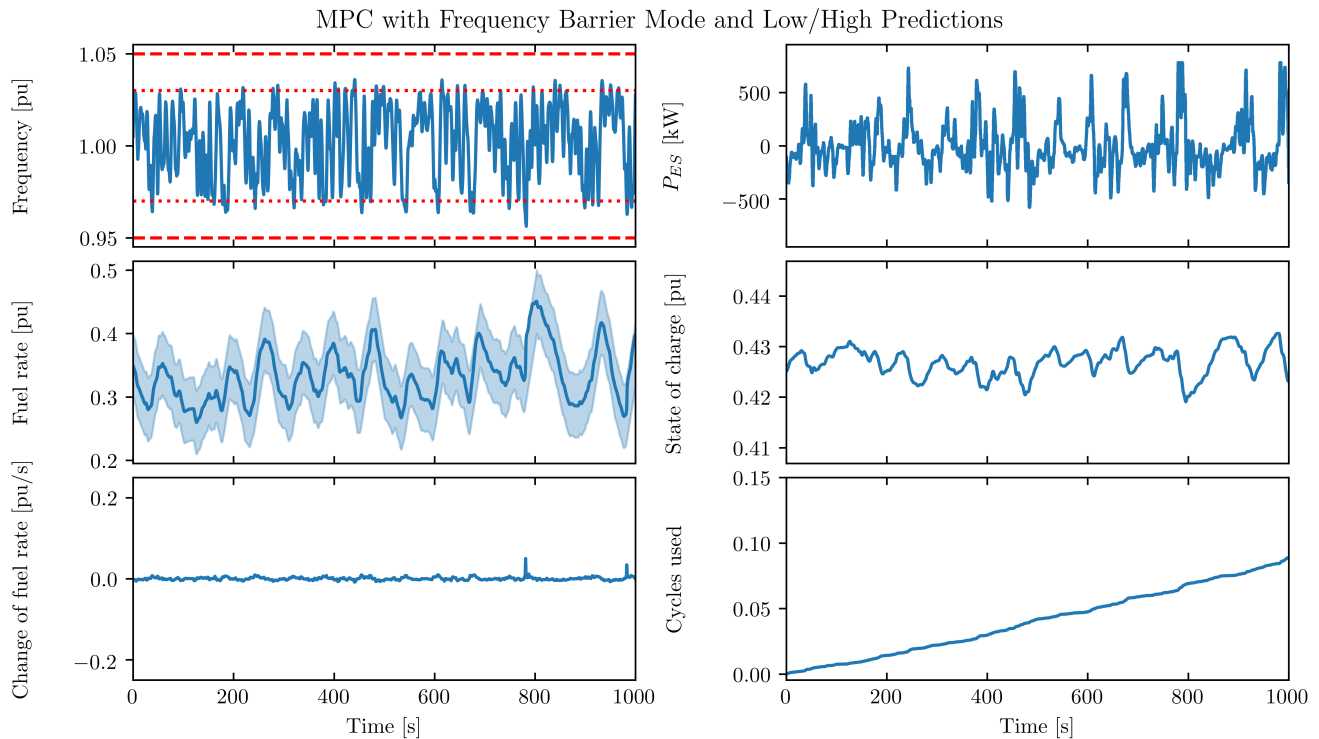


FIGURE 13. Response of the power plant when using the MPC with frequency barrier mode and low/high predictions

The MPC both needs predictions and a model of the plant, this introduces both uncertainty and disturbances. The baseline partly avoids the problem of model uncertainty as the baseline controller does not use any models. However, both controllers are tuned against a modeled plant with its uncertainties. As this is a nonlinear plant it is hard to analytically assess the robustness of the controllers. The baseline controller of the engine inherits the robustness properties of a droop controller, which has proven its robustness as the industry standard for engines in island mode. The MPC includes a terminal cost, this increases the stability property of the controller [39]. The controllers should be thoroughly checked for robustness before use, as it is hard to assess the analytical properties.

B. PREDICTIONS

Two types of prediction are compared for the MPC: low/high prediction and perfect predictions. As expected, it is clear that the perfect prediction performs best. With perfect knowledge, the MPC can optimize the plant for the future load. However, the load is hard to predict. Therefore, the suggested low/high predictions are more realistic. Figure 8 shows typical predictions from the MPC with frequency barrier mode and low/high predictions. Typically, one of the scenarios will be constrained by one of the barriers, while the other is unconstrained (in Figure 8, the low prediction is constrained by the outer frequency barrier).

For both modes, the use of batteries (the number of equiv-

alent full cycles and maximum power) increases when using low/high predictions compared with perfect predictions. This can be seen as a cost of inaccurate predictions.

For the frequency barrier mode, the minimum frequency is slightly decreased with a low/high prediction, but mostly the frequency is kept within the frequency barriers. The variations of the fuel rate are also increased.

The stiff frequency mode is more sensitive to errors in the prediction. As seen in Figure 15, the frequency is not kept constant when the low/high predictions are used. However, by increasing the sampling frequency from 2 Hz to 10 Hz, the MPC is again able to maintain a stiff frequency. The MPC gets information about frequency deviations more often, and can react to them more quickly by increasing the sampling frequency. In contrast, the frequency barrier mode is not as sensitive to frequency deviations, and is therefore more robust to errors in the power prediction.

The performance of the MPC is dependent on good load predictions. Consequently, further work is needed to establish methods for load predictions. This can be models based on the present mode of the vessel and the environment, or it may be black-box models, such as neural network models (e.g. nonlinear auto regressive models).

C. FREQUENCY BARRIER MODE AND STIFF FREQUENCY MODE

The different modes of the MPC may have different use cases. The frequency barrier mode can be used to increase

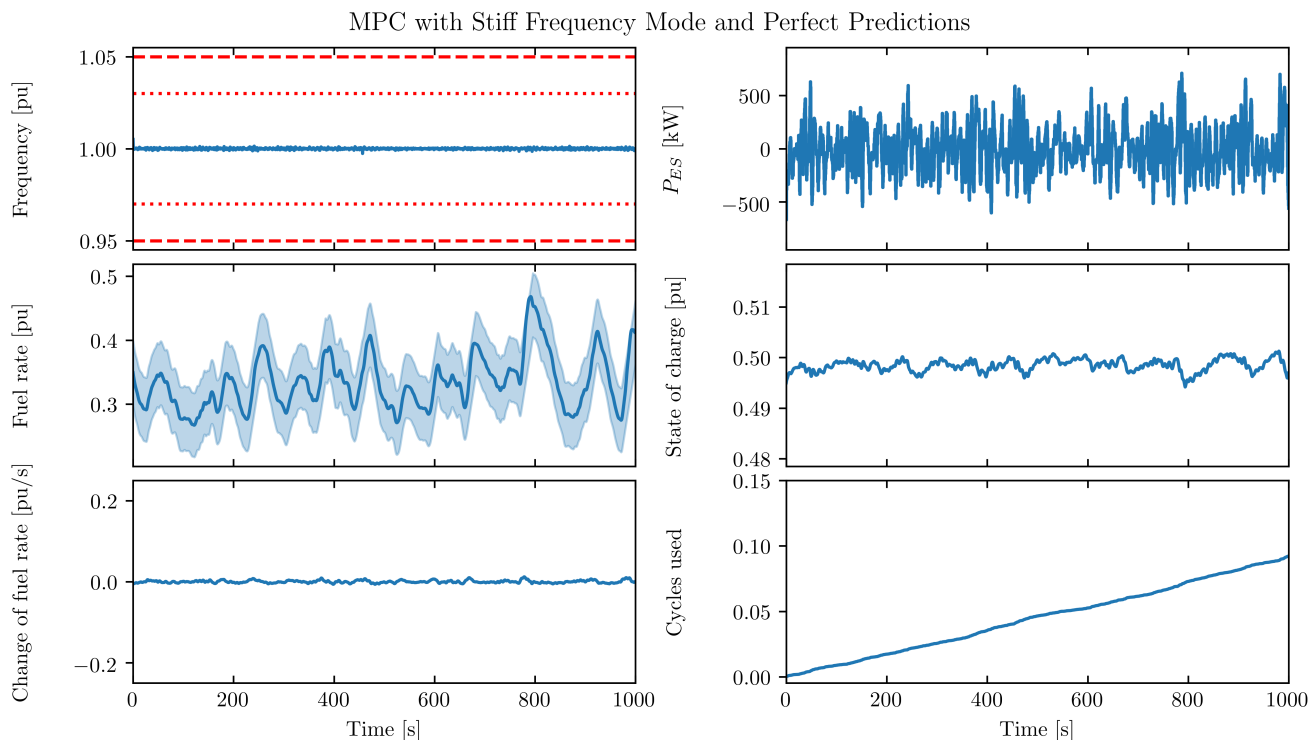


FIGURE 14. Response of the power plant when using the MPC with stiff frequency mode and perfect predictions

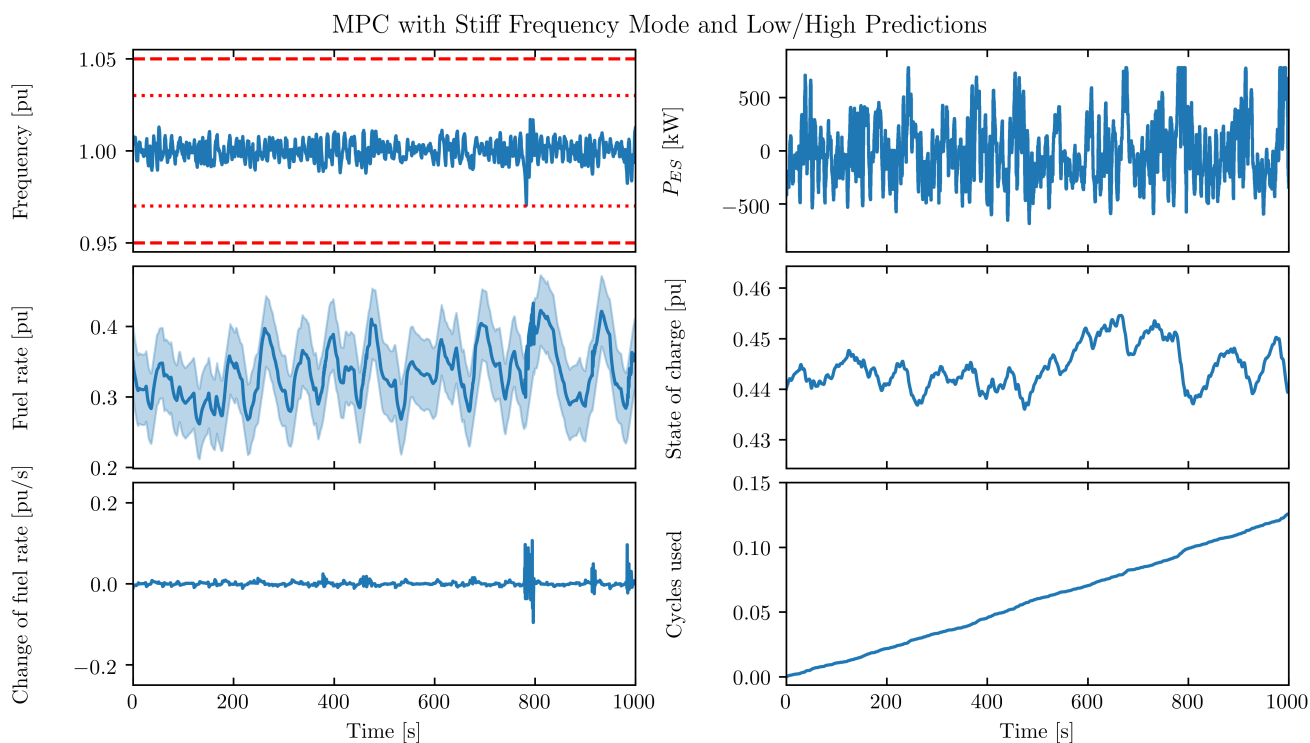


FIGURE 15. Response of the power plant when using the MPC with stiff frequency mode and low/high predictions

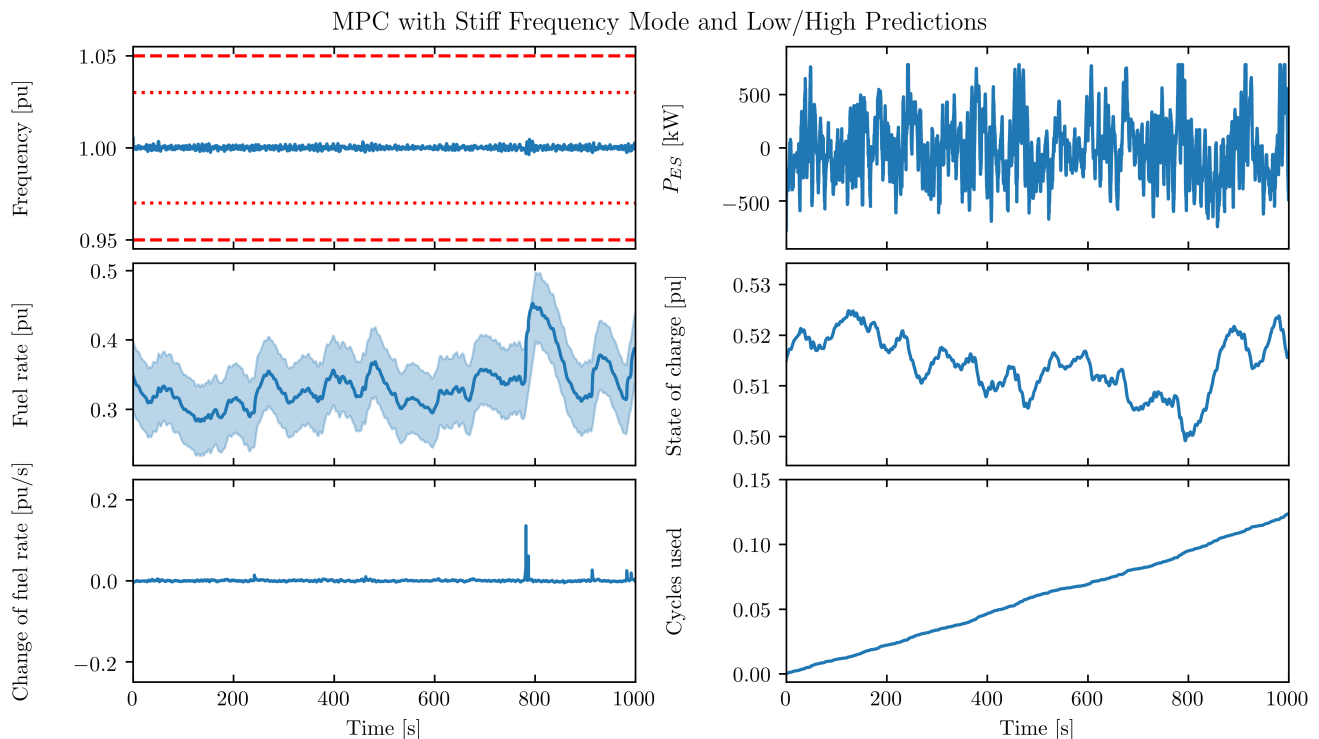


FIGURE 16. Response of the power plant when using the MPC with stiff frequency mode, low/high predictions and an increased sampling frequency (10 Hz)

the performance of the gas engine as the load variations on the gas engine are reduced. In addition, the battery usage is reduced, and the battery may be downsized as the peak power demand is decreased.

The stiff frequency mode may be used when a fixed frequency is needed, which is required when a new generator is synchronized to the grid. For DP operations reliability is highly important. For this reason, the stiff frequency mode may then be preferred. One advantage is that faults may be easier to detect when a stiff frequency is used, as a major deviation of the frequency indicates that a fault exists in the system. Another advantage is that this gives the largest frequency margin, which also gives a safety margin.

D. BATTERY SIZE AND AGING

In Table 3, the number of equivalent full cycles is shown. This is calculated by using the same load series for 10 years. The number of equivalent full cycles is more than three times the rated 12,000 cycles of the battery for many of the modes. However, this is a conservative estimate since the vessel will only be used in harsh DP operations for a short time during the 10 year lifetime of the batteries. In [40], it is reported that the vessel is only in dynamic positioning operations 35% of the time and only a portion of this is in harsh weather. Moreover, the batteries are rated for 15,000 cycles, with a depth of discharge (DoD) of 80% (12,000 equivalent full cycles) [31]. Even so, it is reported that the aging of an NMC cell due to an equivalent full cycle is much larger for a large

DoD, compared with a small DoD [41].

The batteries may therefore be used for additional use cases, such as "spinning reserve." The batteries used in this simulation are able to deliver 780 kW for 20 minutes and can be used to power thruster units during DP operation [29, Pt. 6, Ch. 3., Sec. 8.3]. One usage is that the vessel uses one generator set to produce power, and has a battery ready in backup; this is called "spinning reserve." The battery must then be able to supply sufficient power and energy to safely terminate the current DP operation in the event of a sudden disconnection of the running generator. With this battery, the vessel can run with the battery for "spinning reserve" when the load is small (e.g. in calm weather).

Note that only a small portion of the total energy of the battery is used (max SoC-min SoC). The frequency barrier mode with perfect predictions uses only 1.6 kWh, while the stiff frequency mode with low/high predictions uses 4.8 kWh. The dimensioning factor is therefore the power, not the energy. One alternative would thus be to use ultra capacitors (UC), which have a high power rating, but a low energy capacity. The power capacity of UC is proportional to the voltage. Using 49 UC modules of type "125V Heavy Transportation Modules" from Maxwell gives 5 kWh of useful energy and a minimum power of 794 kW (minimum voltage of 54%) [42]. The weight will be approximately 3,000 kg (slightly less than the 3,800 kg of the suggested battery pack). For the configuration with MPC, the stiff frequency mode and a low/high prediction, 1.46 million equivalent full cycles would be used

by the ultra capacitor. The rated number of cycles is 1 million equivalent full cycles or 10 years of operation.

As noted earlier, the energy buffer of the generator sets is 667 Wh in total. This energy buffer is utilized in the frequency barrier mode. The energy storage requirement is therefore on the order of 3–10 times larger than the kinetic energy storage of the generator set. Note that a larger kinetic energy storage is available if the engines can use a variable frequency (e.g. direct current grid). In these cases, the frequency may vary from 60% to 110%, which increases the kinetic energy storage up to 1.4 kWh. However, at a 60% speed, the power of the engine and generator is reduced to 60% as the torque is limited. Simulation has shown (not presented due to page limitations) that a battery is also needed if the speed can drop to 60%. Typically, a load increase will reduce the speed, and hence the available power, from the generator set. Moreover, a large frequency span can further decrease the number of equivalent cycles.

VI. CONCLUSION

A control method based on model predictive control (MPC) to control an Otto-cycle gas engine and a battery is presented. The controller is compared with a baseline controller, where the generator sets are controlled by speed-droop. For the baseline controller, the battery is controlled as a virtual generator.

The methods are compared by a simulation study, in which a real-world time series of power demand for a DP vessel in a 3 m wave height is used. The MPC is tested with two different power load predictions: either that it uses a high and low scenario for the load, or has perfect knowledge of the upcoming power demand. Two configurations of the cost function are used. One configuration allows the frequency to stay within a band, and has a high cost on the use of the battery. A second configuration has a large penalty on frequency deviations, though use of the battery is cheap.

The simulation shows that the MPC is able to maintain a slowly varying load on the generator set, or keeps the frequency constant if the MPC has perfect knowledge of the upcoming power or a high sample rate is used. The performance is degraded if the future power is unknown. This motivates for further studies on predictions of the short-term power demand of marine vessels.

The lifetime of the battery is also evaluated. The batteries are expected to last for 3 to 10 years of operation with DP harsh weather only. The method seems to be implementable, as the vessel is only in this condition for a small part of the 10-year expected lifetime of the battery.

REFERENCES

- [1] V. Shagar, S. G. Jayasinghe, and H. Enshaie, "Effect of Load Changes on Hybrid Shipboard Power Systems and Energy Storage as a Potential Solution: A Review," *Inventions*, vol. 2, no. 3, p. 21, 2017. [Online]. Available: <http://www.mdpi.com/2411-5134/2/3/21>
- [2] T. W. P. Smith, J. P. Jalkanen, B. A. Anderson, J. J. Corbett, J. Faber, S. Hanayama, E. O'Keefe, S. Parker, L. Johansson, L. Aldous, C. Raucci, M. Traut, S. Ettinger, D. Nelissen, D. S. Lee, S. Ng, A. Agrawal, J. J. Winebrake, and A. Hoen, M., "Third IMO Greenhouse Gas Study 2014," International Maritime Organization (IMO), p. 327, 2014.
- [3] T. Smith, C. Raucci, S. Haji Hosseinloo, I. Rojón, J. Calleya, S. Suarez de la Fuente, P. Wu, and K. Palmer, "CO₂ Emissions from International Shipping: Possible reduction targets and their associated pathways," *Tech. Rep.*, 2016.
- [4] V. Æsøy, P. Magne Einang, D. Stenersen, E. Hennie, and I. Valberg, "LNG-fuelled engines and fuel systems for medium-speed engines in maritime applications," in *SAE International Powertrains, Fuels and Lubricants Meeting*. SAE International, Aug. 2011. [Online]. Available: <https://doi.org/10.4271/2011-01-1998>
- [5] C. Wang, M. H. Nehrir, and S. R. Shaw, "Dynamic models and model validation for pem fuel cells using electrical circuits," *IEEE Transactions on Energy Conversion*, vol. 20, no. 2, pp. 442–451, June 2005.
- [6] B. Zahedi, L. E. Norum, and K. B. Ludvigsen, "Optimized efficiency of all-electric ships by dc hybrid power systems," *Journal of Power Sources*, vol. 255, no. Supplement C, pp. 341–354, 2014. [Online]. Available: <http://www.sciencedirect.com/science/article/pii/S0378775314000469>
- [7] E. Ovrum and T. Bergh, "Modelling lithium-ion battery hybrid ship crane operation," *Applied Energy*, vol. 152, no. Supplement C, pp. 162 – 172, 2015. [Online]. Available: <http://www.sciencedirect.com/science/article/pii/S0306261915001026>
- [8] "Hybrid power system makeover for baltic sea ferry," online, May 2013. [Online]. Available: <http://articles.maritimepropulsion.com/article/Largest-Hybrid-Power-System-in-the-World-Installed-in-Danish-Ferry57461.aspx>
- [9] E. Skjong, E. Rødskar, M. Molinas, T. A. Johansen, and J. Cunningham, "The marine vessel's electrical power system: From its birth to present day," *Proceedings of the IEEE*, vol. 103, no. 12, pp. 2410–2424, Dec. 2015.
- [10] F. Lambert, "Two massive ferries are about to become the biggest all-electric ships in the world," online, August 2017. [Online]. Available: <https://electrek.co/2017/08/24/all-electric-ferries-abb/>
- [11] "A first-hand look at rt adriaan," online, September 2013. [Online]. Available: <http://www.maritimejournal.com/news101/tugs,-towing-and-salvage/a-first-hand-look-at-rt-adriaan>
- [12] "Electric asv awarded," online, June 2017. [Online]. Available: <http://www.maritimejournal.com/news101/power-and-propulsion/electric-asv-awarded>
- [13] "Pioneering battery hybrid ferry launches in fjords," online, July 2016. [Online]. Available: http://www.passengership.info/news/view,pioneering-battery-hybrid-ferry-launches-in-fjords_43774.htm
- [14] "Energy storage systems," online, visited 28.09.2017, 2017. [Online]. Available: <http://new.abb.com/marine/systems-and-solutions/power-generation-and-distribution/energy-storage>
- [15] X. Hu, C. Zou, C. Zhang, and Y. Li, "Technological developments in batteries: A survey of principal roles, types, and management needs," *IEEE Power and Energy Magazine*, vol. 15, no. 5, pp. 20–31, Sept 2017.
- [16] S. Kanerva, P. Pohjanheimo, and M. Kajava, "Dynamic ac concept," *ABB, Tech. Rep.*, 2016.
- [17] J. Hou, J. Sun, and H. F. Hofmann, "Mitigating power fluctuations in electric ship propulsion with hybrid energy storage system: Design and analysis," *IEEE Journal of Oceanic Engineering*, vol. PP, no. 99, pp. 1–15, 2017.
- [18] J. Hou, J. Sun, and H. Hofmann, "Battery/flywheel hybrid energy storage to mitigate load fluctuations in electric ship propulsion systems," in *2017 American Control Conference (ACC)*, May 2017, pp. 1296–1301.
- [19] W. Chen, A. K. Ådnanes, J. F. Hansen, J. O. Lindtjørn, and T. Tang, "Super-capacitors based hybrid converter in marine electric propulsion system," in *The XIX International Conference on Electrical Machines - ICEM 2010*, Sept. 2010, pp. 1–6.
- [20] T. I. Bø and T. A. Johansen, "Battery power smoothing control in a marine electric power plant using nonlinear model predictive control," *IEEE Transactions on Control Systems Technology*, vol. 25, no. 4, pp. 1449–1456, July 2017.
- [21] A. Haseltalab, R. R. Negenborn, and G. Lodewijks, "Multi-Level Predictive Control for Energy Management of Hybrid Ships in the Presence of Uncertainty and Environmental Disturbances," in *14th IFAC Symposium on Control in Transportation SystemsCTS 2016*, vol. 49, no. 3. Elsevier B.V., 2016, pp. 90–95. [Online]. Available: <http://dx.doi.org/10.1016/j.ifacol.2016.07.016> <http://linkinghub.elsevier.com/retrieve/pii/S2405896316302129>
- [22] S. A. M. Al-Barazanchi and A. M. Vural, "Modeling and intelligent control of a stand-alone pv-wind-diesel-battery hybrid system," in *2015*

- International Conference on Control, Instrumentation, Communication and Computational Technologies (ICCICCT), Dec. 2015, pp. 423–430.
- [23] D. C. Das, A. K. Roy, and N. Sinha, “PSO based frequency controller for wind-solar-diesel hybrid energy generation/energy storage system,” in 2011 International Conference on Energy, Automation and Signal, Dec. 2011, pp. 1–6.
- [24] S. Barsali, C. Miulli, and A. Possenti, “A Control Strategy to Minimize Fuel Consumption of Series Hybrid Electric Vehicles,” *IEEE Transactions on Energy Conversion*, vol. 19, no. 1, pp. 187–195, 2004.
- [25] S. M. Lukic, S. G. Wirasingha, F. Rodriguez, J. Cao, and A. Emadi, “Power management of an ultracapacitor/battery hybrid energy storage system in an hev,” in 2006 IEEE Vehicle Power and Propulsion Conference, Sept. 2006, pp. 1–6.
- [26] A. Brahma, Y. Guezennec, and G. Rizzoni, “Optimal energy management in series hybrid electric vehicles,” in Proceedings of the 2000 American Control Conference. ACC (IEEE Cat. No.00CH36334), vol. 1, no. 6, Sept. 2000, pp. 60–64 vol.1.
- [27] E. Vaktskjold, L.-A. Skarbo, K. Valde, K. S. Foer, T. Humerfelt, R. Nordvik, and B. O. Bruvik, “The new bergen B35:40 lean burn marine gas engine serie and practical experiences of SI lean burn gas engines for marine mechanical drive,” Proceedings of the 25th CIMAC Congress. Shanghai, 2013.
- [28] T. I. Bø, A. R. Dahl, T. A. Johansen, E. Mathiesen, M. R. Miyazaki, E. Pedersen, R. Skjetne, A. J. Sørensen, L. Thorat, and K. K. Yum, “Marine vessel and power plant system simulator,” *IEEE Access*, vol. 3, pp. 2065–2079, 2015.
- [29] “Rules for classification: Ships,” DNV GL, Tech. Rep., January 2017.
- [30] PBES, “PBES specification sheet,” Online, visited 28.08.2017., datasheet.
- [31] “Xalt™75 Ah high power (HP) superior lithium ion cell,” Datasheet, September 2014, datasheet number: 09_09_2014_XALT_Energy_75AH_HP_Spec_Sheet.
- [32] T. I. Bø and T. A. Johansen, “Scenario-based fault-tolerant model predictive control for diesel-electric marine power plant,” in 2013 MTS/IEEE OCEANS - Bergen, June 2013, pp. 1–5.
- [33] J. J. May, “Improving engine utilization on DP drilling vessels,” in Dynamic Positioning Conference, 2003.
- [34] A. M. Ersdal, L. Imsland, K. Uhlen, D. Fabozzi, and N. F. Thornhill, “Model predictive load–frequency control taking into account imbalance uncertainty,” *Control Engineering Practice*, vol. 53, no. Supplement C, pp. 139 – 150, 2016. [Online]. Available: <http://www.sciencedirect.com/science/article/pii/S0967066115300496>
- [35] B. Houska, H. Ferreau, and M. Diehl, “An Auto-Generated Real-Time Iteration Algorithm for Nonlinear MPC in the Microsecond Range,” *Automatica*, vol. 47, no. 10, pp. 2279–2285, 2011.
- [36] H. P. Beck and R. Hesse, “Virtual synchronous machine,” 2007 9th International Conference on Electrical Power Quality and Utilisation, EPQU, 2007.
- [37] H. Bevrani, T. Ise, and Y. Miura, “Virtual synchronous generators: A survey and new perspectives,” *International Journal of Electrical Power and Energy Systems*, vol. 54, pp. 244–254, 2014. [Online]. Available: <http://dx.doi.org/10.1016/j.ijepes.2013.07.009>
- [38] Q. C. Zhong and G. Weiss, “Synchronverters: Inverters that mimic synchronous generators,” *IEEE Transactions on Industrial Electronics*, vol. 58, no. 4, pp. 1259–1267, 2011.
- [39] L. Grüne and J. Pannek, *Nonlinear Model Predictive Control*. Springer, 2011.
- [40] T. I. Bø, A. Swider, and E. Pedersen, “Investigation of drivetrain losses of a dp vessel,” in 2017 IEEE Electric Ship Technologies Symposium (ESTS), Aug. 2017, pp. 508–513.
- [41] M. Ecker, N. Nieto, S. Käbitz, J. Schmalstieg, H. Blanke, A. Warnecke, and D. U. Sauer, “Calendar and cycle life study of Li(NiMnCo)O₂-based 18650 lithium-ion batteries,” *Journal of Power Sources*, vol. 248, pp. 839–851, 2014. [Online]. Available: <http://dx.doi.org/10.1016/j.jpowsour.2013.09.143>
- [42] Maxwell, “125v heavy transportation module,” Online, visited 28.08.2017., datasheet, document number 1014696.7.

...